Edinburgh Research Explorer

A model for the spread of fire across a fuel bed incorporating the effects of wind and slope

A Model for the Spread of Fire across a Fuel-Bed

Incorporating the Effects of Wind and Slope

F. MORANDINI·, A. SIMEONI, P.A. SANTONI and J.H. BALBI

Université de Corse, Systèmes Physiques pour l'Environnement U.M.R.-C.N.R.S. 6134

Campus Grossetti, BP 52 20250 Corte, France

Phone: (+33) 495 450 161; Fax: (+33) 495 450 162

Abstract – A two-dimensional non-stationary model of a fire spreading across a bed of fuel is proposed incorporating the effects of wind and slope. The contributions of both radiative and convective preheating ahead of the fire-front are included. The radiation impinging on the top of the fuel-bed is determined, assuming the flame is a radiant surface. Convective heat transfer in the fuel layer is considered using a simplified description of the flow through the bed of fuel. Dedicated laboratory-scale experiments have been carried out across beds of pine needles for horizontal fire spread in still air, in order to validate the model. Experiments conducted under wind and slope conditions are also considered. Model predictions are then compared to these experimental measurements.

· Corresponding Author. Email: morandin@univ-corse.fr

INTRODUCTION

Wind and slope are two environmental factors affecting dramatically the rate of spread of a fire and determining how much energy is transferred towards the unburned fuel via radiation and convection. The effects of wind velocity and/or slope on the spread of a fire have been widely studied experimentally (Dupuy, 1995; Weise and Biging, 1997; Catchpole et al., 1998; Mendes-Lopes et al., 1998), but few models include both these variables. These environmental factors can be incorporated in models of fire spread in various ways. Modelling approaches based on fundamental conservation equations (Grishin, 1997; Larini et al., 1997; Linn and Harlow, 1998; Margerit and Séro-Guillaume, 2002) intrinsically take into account the effects of wind and slope. The different modes of heat transfer can be quantified but, these models are computationally intensive. In empirical models used in fire management tools (Rothermel, 1972), the influence of the ambient wind or slope are taken into account using coefficients to modify the propagating heat flux. This consists in incorporating multipliers of fire rate of spread expected in the absence of wind and slope. A review of such models (Weise and Biging, 1997) indicates that reasonable results can be obtained with the various methods used to combine the effects of wind and slope.

Numerous authors have emphasised the analogy which can be drawn between the effects of wind and slope (Fons, 1946; Rothermel, 1972; Cheney, 1981; Weber, 1989; Viegas, 1994). Thus, the effects of wind for instance, can also be included in a model of fire-spread incorporating the effects of slope by means of an equivalent slope (or *vice versa*) but the range of application is limited. In previous works, a model of fire spreading across a sloping surface has been developed (Morandini et al., 2001a). Radiation from the flame was supposed to dominate heat transfer, assuming the flame to be a radiating surface. Next, generalisation to the fire spread under wind-blown

conditions was presented on the basis of the assumption that the effect of wind was similar to that of the slope (Morandini et al., 2001b). The increase in rate of spread with increasing wind was attributed to increased radiation impinging on the top of the fuel-bed due to the tilted flames: wind and slope, which cause the same degree of flame tilt, lead to the same rate of spread. The results were in good agreement with experimental data for low wind velocity but the model underpredicts the rate of spread for greater wind velocity. The reason for this discrepancy was due to the absence of convective heat transfer mechanism, the influence of which becomes significant with increasing wind velocity.

In a parallel work, the wind-aided spread of a fire has been investigated (Simeoni et al., 2001). Along similar lines, a theoretical study has been undertaken to improve the fire-spread formulation. The concept involved reducing the multiphase model developed by Larini et al. (1997) and deriving a set of equations which were compared to our formulation. The convective heat transfers, missing in our model's energy conservation equation, were then incorporated (Simeoni et al., 2002). A simplified flow model through the fuel layer was also coupled to the fire spread formulation. Nevertheless, radiative transfers from the flame were poorly represented and this formulation did not provide an adequate basis for describing correctly the combined effects of steep slope and high wind.

In the present work, we merge the two previous approaches (Morandini et al., 2001b; Simeoni et al., 2003) as a further step towards our long-term goal of providing a fire management tool. So far, such tools have been developed from empirical or statistical models only. Approaches based on fundamental conservation equations are computationally intensive, and simpler models with time-saving numerical resolution, are required. The fire rate of spread, the fire-front geometry and the temperature field in

the fuel layer are the main features which have to be predicted. A satisfying solution can be found in simplified models based on both modelling and experimental data. Review of the literature confirms that models combining empiricism and theory are probably better than using either independently and should therefore be preferred (Steward, 1974; Viegas, 1998). Some modelling approaches are developed in this way (Vaz et al., 2002 Catchpole et al. 2002) but these formulations assume the fire front as an infinite straight line and only consider heat transfers in the fuel bed ahead of the fire font, unlike the model presented in this paper that describes the heat transfer in the whole domain of spreading and that provides the fire front perimeter.

The model predictions are compared to laboratory-scale measurements for the spread of a fire across beds of pine needles. Specific experiments have been carried out for horizontal fire spread in still air in order to measure flame front and fire front properties using an infrared camera, thermocouples and heat flux sensors. Indeed, for models based on the energy conservation equations, the temperature agreement with experimental data is not enough and the contributions of the predicted heat fluxes (radiant and convective) have to be checked too. Laboratory-scale experiments conducted under wind and slope conditions are also considered. Comparisons between predicted and observed rate of spread and temperature-time curves are presented for several wind and slope configurations. Simulated effects of wind and slope on the fire-front shape, the gas velocity components within the fuel bed and the heat flux contributions are discussed.

FIRE SPREAD EXPERIMENTS

Horizontal Fire Spread in Still Air

Experimental fires were conducted at the University of Corsica laboratory in a closed room without any air motion. The series of experiments were carried out on a dedicated combustion table across pine-needle beds (Morandini et al., 2002; Santoni et al, 2003). They were performed in order to measure flame front and fire front properties for horizontal spread in still air.

The combustion table, made of wood and insulated on the top surface with a special light refractory cement, is 1.5 m long and 1 m wide. The bed of fuel occupies only the central part of the tray (0.5 m wide) and consists of a layer of *Pinus pinaster* needles with a load of approximately 0.5 $kg.m^{-2}$ on a dry basis. The pine needles drying process is archived in an oven kept at a constant temperature of $60°C$ during 24 hours. The ratio of area to volume and density are 4550 m^{-1} and 680 kg/m^3, respectively. The depth of fuel was approximately 2.3 cm, giving a bulk density of 21.74 kg/m^3 and a packing ratio of 0.032. The ambient temperature was about $28°C$ during experiments.

The conditioned pine needles are scattered uniformly on the tray. To ensure fast and linear ignition, a small amount of alcohol and a flame torch are used. Eight runs have been carried out. Smoke was removed from the room after each test.

Thermocouples

The first set of K-type thermocouples are located above the fuel sample along the vertical direction. The temperature measurements are made, in the centre of the fuel bed, both in the flame and plume regions by using double thermocouple probe technique (Santoni et al. 2001, Marcelli et al. 2002). A probe is composed of a two holes insulator. The thermocouples were threaded through these holes and their

junctions were set at a distance of about 0.3 *mm* from each other. At the exposed hot junctions the wires were 50 and 100 *μm* in diameter respectively. A technique, which consists in compensating the temperature provided by the thermocouples when the probe is immersed in a flame in order to restore the dynamic of the signals (Santoni et al., 2002), was used. This technique necessitates a high acquisition rate (700 measurements per second). A double thermocouple probes array was installed above the fuel bed. The measuring section is located approximately 0.35 *m* before the end of the fuel bed. This positioning was far enough from the ignition line for fire to achieve a constant rate of spread and flame front shape when it passed through the thermocouples. A supporting rod, set perpendicularly to the tray surface, was prepared to hold 8 of these probes. Measurement heights were 0.04, 0.06, 0.08, 0.12, 0.16, 0.20, 0.24 and 0.28 *m* from the tray surface. Moreover, the gas velocity has been derived by using the cross-correlation of random thermal fluctuations (Santoni et al. 2001).

The second set of thermocouples is located inside the bed of pine needles along the horizontal direction. Six K-type thermocouples with 100 *μm* wire diameter, spaced 0.07 *m* apart and positioned in the centre of the fuel bed, allowed the temperature of the litter to be recorded. The first thermocouple was located 0.20 *m* from the beginning of the bed of fuel. Only these temperature measurements inside the fuel bed, will be considered hereafter for comparison with the predictions of the fire spread model. The sampling rate was 25 measurements per second.

Infrared camera

The experimental runs are recorded with an a MWIR (3-5 *μm*) Focal Plane Array infrared camera (CEDIP, Jade3MW). The acquisition frequency is 25 images per seconds. Each infrared image is composed of 256×256 pixels and the digital level of a

pixel has a 14 bits resolution. Digital images are stored on a PC. The two following kinds of measurements have been done with two different special filters.

- During combustion process in the gaseous phase, the major part of the products emits radiation in the infrared region and more intensively in the 4.3 μm band due to the asymmetric stretch vibration of CO_2 molecules. In order to obtain measurements of the buoyant diffusion flame properties, the camera using a filter for CO_2 species (specified wavelength near 4.3 μm), was located in front of the flame front at the end of the bed. The figure illustrate the position of the camera with an example of the field of view. Only qualitative measurements of buoyant diffusion flame characteristic length scales have been done using infrared image processing technique (Morandini *et* al., 2002). The emissivity of the semi-transparent media is not easy to determine and thus the images obtained are not calibrated. The continuous flame length, L_c and the maximum flame length, L_m allow to determine the limits between three regions: the continuous flame region is found below L_c, the intermittent is found between L_c and L_m and the plume region is found above L_m. The average flame length was used as an input of the model to determine the radiation from the flame front impinging on the top of the litter. These characteristic length scales, can also be used with empirical correlations to determine centreline temperature and velocity distributions along the vertical direction (Morandini *et al*., 2002).

- Quantitative measurements of the temperature of the bed of fuel have been done assuming pine needles as black-body ($\varepsilon = 1$). In this case, a filter to eliminate the CO_2 and H_2O radiation and make high temperature measurements (specified wavelength near 3.9 μm), was used. With such filter, the calibrated camera is capable of measuring temperature in the range of 200°C to 1100°C. The camera

was located at a height of 2 meters and set perpendicularly to the fire spread. The figure illustrate the position of the camera with an example of the field of view. The rate of spread is obtained from the derivative of the curve *"flame front position vs time"*.

Heat flux sensors

Radiation and convection are commonly invoked as being the dominant heat transfer mechanisms responsible of the rate of spread, but few data are available in the literature. These specific experiments have been carried out to measure the contribution of convection and radiation, in order to validate the model predictions. Two heat flux sensors were located at the end of the bed of pine needles and the normal of their sensing area were vertically oriented in order to measure heat fluxes from the flame front impinging on the top of the litter (figure). The two sensors used incorporate balanced thermoelectric panels housed between cooper foils which provide low response time lower than 0.5 s. Each of these hemispherical sensors is composed of two different sensing areas (squares of 1 cm^2) on a heat exchanger. They are capable of measuring either radiant and convective or convective and total heat fluxes up to 100 kW/m^2. The sensibility of the sensors is provided in table 2.

Wind-blown fire spread across a sloping surface

In addition, complementary series of experiments carried out across the same beds of pine needles in a dedicated low speed wind tunnel at the *Instituto Superior Técnico* of Lisboa (Mendes-Lopes et al., 1998; Ventura et al., 1998) will be also compared to model predictions. They were performed in order to observe wind-driven fire across pine-needle beds. In addition, the tunnel makes it possible to study the effects of slope by

means of a sloping fuel tray. The wind speed values covered the range between -3 $m.s^{-1}$ and 3 $m.s^{-1}$. The movable tray can be set at angles from 0 up to 15° with up-slope and down-slope orientation. The average values of flame length and tilt angle used as model input for flame radiation calculation are provided in figure 4.

FIRE SPREAD FORMULATION

The model represents the merging of the radiative approach (Morandini et al., 2001b) with the advective one (Simeoni et al., 2003), in order to represent the whole heat transfers occuring in the fire spread under combined slope and wind conditions.

Fire spread thermal balance

To set the thermal balance on a medium equivalent to the gas and solid complex, we set the following assumptions (Simeoni et al., 2003):thermal equilibrium between the gaseous and solid phases, constant gas specific heat at constant pressure and uniform profile along the vertical in the fuel layer for the state variables (except for the gas horizontal velocity component). Then, we obtained the following equation, taking into account heat transfer mechanisms for total depth control volumes.

$$\frac{\partial T}{\partial t} + k_w \vec{V}_g . \vec{\nabla} T = -h(T - T_a) + K\Delta T + R - Q\frac{\partial \sigma_k}{\partial t} \quad \text{on the fuel complex,} \tag{1}$$

$$\sigma_k = \sigma_{k_0}, \quad R = \frac{a_k}{m} \varepsilon_{fl} B T_{fl}^4 \int_{S_{fl}} \frac{\cos\varphi_{fl} \cos\varphi_k}{\pi r^2} dS_{fl} \quad \text{for unburned cell ahead of the front,} \tag{2}$$

$$\sigma_k = \sigma_{k_0} e^{-\gamma(t - t_{ig})}, \quad R = 0 \qquad\qquad \text{for a burning cell,} \tag{3}$$

with the following boundary and initial conditions:

$$\vec{n}.\nabla T = 0 \qquad\qquad\qquad \text{at the fuel-bed boundaries,} \tag{4}$$

$$T_0 = T_a \qquad\qquad\qquad \text{for an unignited cell at time zero,} \tag{5}$$

$$T_0 = T_{ig} \qquad\qquad\qquad \text{for an ignited cell at time zero.} \tag{6}$$

Heat transfer and production processes in the thermal balance (Equation 1) are determined as follows:

- The gaseous phase velocity in the fuel layer, which determines forced convection heat transfer, is obtained by a simplified flow model (detailed hereafter). The parameter k_w is deduced from the reduction of the multiphase model and depends on the equivalent medium properties (Simeoni et al., 2001):

$$k_w = \frac{\alpha_g \; \rho_a \; \delta \; C_{p,g}}{m} \cdot \frac{T_a}{T} \tag{7}$$

- The energy exchanged between a control volume and the surrounding air is assumed to be proportional to the difference between the temperature of this volume and the ambient temperature.

- The heat transferred between a control volume and its neighbouring in the burning zone located inside the litter is mainly due to embers radiation. These exchanges are assumed to be represented by a single diffusion term.

- The flame is modelled as a radiant surface with a given height and constant temperature T_{fl} and emissivity ε_{fl}. The flame height is supposed to be known *a priori* and it is assumed to be equal to half of the maximum flame height. The flame temperature is assumed to be equal to that of the combustion zone (provided by the model of fire spread). The flame tilt angle is derived from empirical correlation (ref). The amount of radiative energy impinging on the top of the litter is determined by means of the Stefan-Boltzmann law. This law makes it possible to determine the part of radiation emitted from an element of the flame front of area dS_{fl}, which impinges on unburned fuel element dS_k (Morandini et al., 2001b). This amount of energy is attenuated according an inverse square law of the distance r between the two areas and also depends on the cosine of angles φ_{fl}

and φ_k defined between the ray and the normal of dS_{fl} and dS_k, respectively (Figure 1). The rate at which the radiant energy from the flame-front is absorbed by the fuel element dS_k is:

$$\phi_{fl-dk} = a_k \, \varepsilon_{fl} \, B \, T_{fl}^4 \int_{S_{fl}} \frac{\cos\varphi_{fl} \, \cos\varphi_k}{\pi \, r^2} \, dS_{fl} \, dS_k \tag{8}$$

where integral over S_{fl} is over the flame surface, B is the Stefan-Boltzmann constant, a_k is the fuel-bed coefficient absorption and ε_{fl} is the flame emissivity. Thus, the parameter R represents the ratio of the radiant heat flux from flames intercepted by the fuel to the thermal mass of the fuel per unit area

$$R = \frac{\phi_{fl-dk}}{m \, dS_k} \tag{9}$$

- The combustion reaction is assumed to occur above a threshold temperature, T_{ig}, the value of which, for forest fuels, is commonly assumed to be 300°C. All the solid degradation processes (drying, pyrolysis and char combustion) as well as the combustion in the gaseous phase are assumed to be represented by a single simplified exothermic reaction. During reaction, the fuel mass is assumed to decrease exponentially,

$$\sigma_k = \sigma_{k_0} \, e^{-\gamma(t-t_{ig})} \tag{10}$$

The model parameters (h, K, Q and γ) are determined from a measured time-temperature curve obtained for a linear spread under no slope and no wind conditions following the method proposed in Balbi et al. (1999). They are identified once for a given fuel and fuel load and remain valid for all the experiments considered hereafter, whatever the slope and wind. The model parameters for fire spread across a 0.5 kg.m^{-2} load of *Pinus pinaster* needles are given in Table 1.

Simplified flow formulation

The gas velocity in the fuel layer needs to be known to determine the advective term present in equation 1. A sub-model of simplified flow was developed in this way by reducing a multiphase formulation (Simeoni et al., 2003). In order to describe fully the aerodynamics, the whole set of equations governing the flow should be considered. In accordance with our aim to represent the phenomena in a simple way, local wind variations are described by taking into account mainly the effects of buoyancy induced by the combustion in the burning zone (Figure 2). As a first step, a one dimensional approach was developed, taking into account the flow in the direction of the slope only, which corresponds to the experiments considered. This formulation is based on simplified mass balance and momentum equation.

The following equations describe the flow through the porous bed of fuel:

$$\frac{\partial V_{g,x}}{\partial x} + \frac{V_{g,x}}{\rho_g}\frac{\partial \rho_g}{\partial x} = -\frac{V_{g,z}(\delta)}{\delta} - \frac{1}{\rho_g \delta}\frac{\partial \sigma_v}{\partial t} \qquad \text{in the burning zone} \qquad (11)$$

$$V_{g,z}(\delta) = \chi\sqrt{2\delta\left(\frac{T}{T_a}-1\right)g\,\cos(s)} \qquad \text{in the burning zone} \qquad (12)$$

$$\rho_g T = \rho_a T_a \qquad \text{in the gas phase} \qquad (13)$$

where χ is a drag forces coefficient (Simeoni et al., 2003). The gas density ρ_g is defined by using the isobaric perfect gas law (Eq. 13) assuming the thermal equilibrium between the gaseous and solid phases in the fuel layer. So the gas density is obtained directly from the temperature provided by the thermal balance.

The domain of validity of the simplified equations was limited to the combustion zone. Equation 12, providing the vertical component of the velocity at the top of the bed of fuel, was obtained for a momentum equation assuming that buoyancy effects dominate the other effects. This hypothesis is only valid in the combustion region where

the calculation of the local wind is performed. Outside this zone, horizontal velocity is supposed to remain constant and equal to the velocity obtained at the boundaries.

Numerical method

The solid phase equations are discretized on a uniform rectangular grid using the finite difference method. An "upwind" difference schema was used to take into account the extent of convective transfers in the wind direction. The resulting system of linear algebraic equations is then solved using the Jacobi iterative method. The gaseous phase equations were solved using a 4th order Runge-Kutta method, assuming a quasi-static flow. The mesh size was *0.01 m* and the time step was in the range of 0.01 s and 0.002 s for the wind velocities considered.

RESULTS AND DISCUSSION

We compared the model with experiments twice. It corresponds to the two experiments presented here before. The first one, conducted for horizontal fires in still air, was finely instrumented and allowed a large quantitative comparison. The second one, conducted in the wind tunnel of the IST was less instrumented, then we will discuss some results of the model in a qualitative way.

Horizontal Fire Spread in Still Air

Fire spread across an horizontal surface in still air will be considered hereafter. First, the infrared camera was used to determine the centreline temperature in the flame front along the vertical direction thanks to correlation established by McCaffrey (1979). These temperatures are compared to thermocouples measurements in the gaseous phase and the radiant panel assumption. Next, the predictions of the temperature of the fuel-

bed are compared to thermocouples and infrared measurements. Finally, the heat fluxes impinging ahead of the fire front are discussed.

<u>Image processing technique</u>

A filter for CO_2 species (4.3 *μm*) was used with the infrared camera. The different steps of the combustion process of the fuel sample located in the measuring section, was recorded. The field of view of the infrared camera is provided in figure 4.a. Three runs of horizontal fire spread across a load of 0.5 *kg.m⁻²* of *Pinus pinaster* needles were recorded. In order to obtain the two flame characteristic length scales, an image processing technique was derived from image processing of video recordings (Audouin et al. 1995). The image processing technique is based on a binarization of the infrared images. It consists in assigning a threshold value of the digital level of the pixel DL_b below which the flame is considered to be absent.. For this work the value of DL_b of 5000 is considered to describe best the flame. Below DL_b the flame is considered to be absent and a value of 0 is assigned to the pixels; above this threshold flame is considered to be present and a value of 1 is assigned to the pixels.

The flame characteristic length scales for the series of experiments conducted across pine needles bed are extracted from these infrared images by using the previous image processing technique. Fire front across an horizontal surface exhibits a quasi-linear shape during spread. This technique was applied to 150 images of the fully developed buoyant diffusion flame when the flame front enters in the measuring section (location of the first set of thermocouples). By averaging all binarized images, the intermittency of flame length (Zukoski 1995), which represents the flame presence probability contours, is obtained (figure .a). The continuous flame length L_c is defined as the distance from the bed of fuel at which the flame intermittency is 0.95 and the maximum

flame length L_m is defined as the distance from the bed of fuel at which the intermittency is 0.05. The continuous flame region is found below L_c, the intermittent is found between L_c and L_m and the plume region is found above L_m. Another important characteristics length scale defined by Zukoski et al. (1984) is the average flame height, L_f which is defined as the height for which intermittency is 0.50. The vertical distribution of the presence probability for the flame zone located at the centre of the fuel bed (dashed line in figure .a) is provided in figure .b. The value of L_c and L_m, for the flame zone located at the centre of the fuel bed are 0.11 and 0.31 cm, respectively. The mean flame height L_f is found to be about 0.21 cm.

Centreline temperature and velocity distributions

The following empirical correlations have been established by McCaffrey (1979), for diffusion pool flame, to describe the centreline temperature and velocity distributions in the three flame regions:

$$\frac{2g\Delta T}{T_0} = K_T \left(\frac{z}{Q^{2/5}} \right)^{2\eta-1} \tag{14}$$

$$\frac{V}{Q^{1/5}} = K_V \left(\frac{z}{Q^{2/5}} \right)^{\eta} \tag{15}$$

where g is gravitational acceleration, ΔT is temperature rise above the ambient, T_0 is ambient temperature, V is vertical flow velocity, η is exponent of centreline correlations, K_T is coefficient for centreline temperature, K_V is coefficient for centreline velocity correlation, z is vertical height above fuel bed and Q is heat release rate.

Following the work of Audouin et al. (1995), K_T and K_V can be determined from characteristic length scales, namely L_c and L_m. The values of these empirical coefficients are provided in Table 3. The previous relations where established for a square burner and we propose test the validity of this approach for a line source.

The fuel mass, $\dot{m}$ and the heat of reaction, Hc were $0.44\,g/s$ and $21000\,kJ/kg$, respectively. The heat release rate, Q is commonly used to characterize flames and is obtained by multiplying the two previous quantities. For the present experiments conducted across pine needles bed, the heat release rate was about $9\,kW$.

The characteristic length scales determined previously are used with McCaffrey empirical correlations to determine centreline distributions in the three flame regions. The temperature distribution is presented in Figure 6. Experimental data and predictions are represented with symbols and solid line, respectively. The agreement between predicted centreline temperature distribution and experimental data is good in the continuous and intermittent flame regions. The characteristics slope coefficient η, defined by McCaffrey is conserved for a line fire spread across pine needles bed. The maximum probe height ($0.28\,m$) was not sufficient to allow measurements in the plume region.

In the model, the radiant panel temperature was assumed to be independent of height, and its length was assumed to be equal to half of the maximum flame height and the flame temperature was assumed to be constant (figure). Nevertheless, the order of magnitude of the temperature, supposed to be equal to that of the combustion zone provided by the model of fire spread, is also satisfying.

Fuel bed temperature

A filter used to eliminate the CO_2 and H_2O radiation and make high temperature measurements (specified wavelength near $3.9\,\mu m$), was used with the infrared camera. The field of view of the infrared camera is provided in figure 4.b. Four runs of horizontal fire spread across a load of $0.5\,kg.m^{-2}$ of *Pinus pinaster* needles were

recorded. The pine needles was considered as black bodies. The temperature of the fuel bed is determined assuming the litter to be a surface with emissivity equal to unity.

The temperature measured with the camera is compared to the data provided by the second set of thermocouples located inside the bed of fuel. Results for two thermocouples locations (x = 0.20 m and x = 0.27 m) are provided in Figure. The measured (infrared and thermocouple) temperature-time curves are also compared to predictions. The infrared camera, calibrated for an integration time of 50 μs, allows to measure accurately temperature of the fuel bed ranging from 200 to 1000°C, and only the temperature of the pine needles during pyrolysis and char combustion will be considered hereafter. Indeed, in this configuration the camera sensibility between 30 and 200°C is not sufficient to provide accurate measurements in this range of temperature; this explain the overestimation of the temperature during preheating and cooling.

In previous works (Balbi et al., 1999; Santoni et al., 1999) 1 mm gauge wire thermocouples were used and the following important feature of the fire spread could not be observed. The infrared images and the temperature measured with 100 μm thermocouple wires, show the presence of two fire fronts : a gaseous combustion zone delimited by the pyrolysis front (first temperature peak) and a char combustion zone (second temperature peak). Between these two high temperature zones, there is a colder one. In this last zone, all the oxygen is consumed in the gaseous phase combustion and char combustion can not occur in oxygen-poor atmosphere.

The measured temperatures are different during pyrolysis since the thermocouple measure gaseous phase temperature whereas the camera measure the fuel bed temperature. The thermal equilibrium between gaseous and solid phases in not achieved during pyrolysis. The temperature of the pine needles is lower since pyrolysis is an

endothermic reaction. The temperature measured with the infrared camera matches the one measured with the thermocouples during char combustion since the black body assumption is fully justified. The ashes temperature measured with the infrared camera is overestimate during cooling due to the insulated material inertia.

The model predictions account accurately of fuel preheating ahead of the flame front. Nevertheless, the simplified formulation of the degradation processes of the solid phase do not allow to distinguish the pyrolysis and char combustion, represented as a single reaction.

Heat fluxes

A quantitative study of heat fluxes (radiation and convection), received ahead of the fire-front at the centreline of the bed, is provided hereafter. In figure, predictions are compared to measurements, where experimental data are deduced from heat fluxes versus time measurements assuming the fire front to be a steady combustion wave : the rate of spread was 2.5 $mm.s^{-1}$.

The order of magnitude of the radiant heat flux emitted from flames impinging on the top of the bed of fuel, agrees with experimental measurements conducted on bed of pine needle for static fires (Dupuy et al., 1998). Impact of radiation acts over a great distance from the fire-front. The distance of preheating of the unburned fuel located ahead of the fire-front is about 0.20 m. The predicted radiant heat flux is close to experimental measurements and this explains the temperature agreement during preheating.

On the other hand, the amount of energy transferred through the bed of fuel by convection is received closer to the front. The convection heat flux predicted model.

The contribution of the diffusion term in the energy conservation equation is significant close to the front (rajouter sur le schema).

Wind-Blown Fire Spread across a Sloping Surface

In the current section, both wind velocity and slope are considered for different combinations of their value. The following configurations have been studied: wind-driven up-slope fires for wind and slope ranging from 0 to 3 $m.s^{-1}$ and 0 to 15°, respectively. First, the rate of spread and the temperature time predictions are compared to laboratory scale measurements (Mendes-Lopes et al., 1998; Ventura et al., 1998). Next, predictions of the effects of wind and slope on the fire-front shape, the velocity components and the heat flux contributions are also discussed.

Rate of spread

The predicted rate of spread is first provided in Figure 5.a for horizontal spread and wind velocity ranging from 0 to 3 $m.s^{-1}$. Predictions, in agreement with experimental data, show that the fire rate of spread increases with increasing wind velocity. Heat transfers by convection inside the litter increase with increasing wind velocity. Furthermore, wind-driven flames lean forward increasing the radiative heat transfer toward the unburned fuel. The fraction of the total energy transferred by flame radiation and convection will be discussed in the following section when the respective contributions of each heat transfer mechanism are presented.

The comparison between the predicted rates of spread and observations for wind-driven 10° up-slope fires are provided in Figure 5.b. The model predictions show that the effect of slope further enhances the fire rate of spread increase with increasing wind velocity, in accordance with observations. It should be noted that the turbulent nature of the flow can explain the scattering of the measured rates of spread for a 3 $m.s^{-1}$ wind velocity.

In order to collate the whole set of configuration results, predicted *versus* average observed rates of spread are given in Figure 6 for up-slope and wind velocity ranging from 0 to 15° and 0 to 3 $m.s^{-1}$, respectively. In the present work, convective heat transfer mechanisms are considered and the model can account for the rate of spread for greatest wind velocity. Overall agreement between the predicted and measured rate of spread is good except for the most extreme configuration, namely for the 3 $m.s^{-1}$ up-wind fire spread across a 15° up-slope surface for which data scattering was marked due to random direct contact of the flame onto the top of the fuel-bed. For this extreme configuration, a mixed flow boundary layer, which was not considered in our modelling approach, developed above the bed of fuel and considerably increases radiative and convective transfers impinging upon the fuel-bed surface.

Temperature-time curves

The predicted and measured temperature-time curves for a 10° up-slope fire spread across a load of 0.5 $kg.m^{-2}$ of Pinus pinaster needles are provided in Figure 7 for 1 and 2 $m.s^{-1}$ wind velocity. It should be noted that obtaining reproducible temperature-time measurements is not easy for wind-blown fires. The differences between experimental runs are mainly due to the highly turbulent aspect of the flames under wind conditions and its geometrical and dynamic characteristics.

These time-temperature curves confirm that the fire travels faster when wind velocity increases. The time for the unburned fuel to ignite is shorter when wind velocity increases: the preheating time for 1 and 2 $m.s^{-1}$ wind velocity is about 50 and 30 s, respectively. The model predictions are in agreement with this tendency.

In our previous works (Santoni et al., 1999; Simeoni et al., 2001), certain aspects of the fire behaviour were not predicted. For instance, the temperature field ahead of the

fire-front was not accurately predicted since the amount of radiative transfer was assumed to prevail over a short distance and in a single direction. In the present study, the temperature predictions are in good agreement with measurements during temperature rise up to ignition. Furthermore, the long range preheating mechanism by radiation and convection appears to be an important feature of up-slope and wind-blown fires and will be discussed hereafter when convective and radiative contributions are considered. With regard to the maximum temperature zone, namely in the flame, it is not accurately described by thermocouple measurements since no correction technique was applied (Santoni et al., 2002) and comparison to prediction is not easy. Furthermore, the simplified combustion modelling does not take into account the wind influence on reaction kinetic bringing more oxygen into the combustion area. A previous study showed that the inclusion of this phenomenon in our modelling is of a great interest (Simeoni et al., 2002); but it was in an empirical way, so it is not possible to include it in the present model yet. Nevertheless, it should be noted that measurements obtained using infrared thermal imaging (Den Breejen et al., 1998) yielded maximum temperatures (approximately $1200°C$ for needle beds of the same type as those used in this study) which corresponds to the temperatures generated by the model.

<u>Fire-front shape</u>

The predicted fire-front shapes for 1 and 2 $m.s^{-1}$ wind-blown fires are provided in Figure 8 at times 100 and 55 s, respectively. When, quasi-steady state is reached, it should be noted that fire travels faster near the centre of the bed of fuel than on the edge since the amount of heat input is greater there. The effects of wind and slope further enhanced fire-front shape distortion. Moreover, the fire-front depth increase with

increasing wind velocity is also depicted. Observed fire-fronts, which exhibit the same tendencies, have not been digitised and comparisons with predictions are not provided here.

Velocity components inside the bed of fuel

The spatial distributions of the predicted horizontal and vertical gas velocities at the centreline of the bed of fuel, for a 10° up-slope fire spread for 1 and 2 $m.s^{-1}$ wind velocity are presented in Figure 9 at times 100 and 55 s, respectively. These distribution patterns occur when the fire-front has travelled about 1.5 m along the combustion table and the quasi-steady state is reached (Figure 8). The gas velocity components will be qualitatively examined here because of the lack of measurements in the combustion zone.

Ascensional velocity is maximal in the combustion zone and was very low outside this zone. The gas behaviour is thus qualitatively described and the order of magnitude of the maximum is correct compared to experiments (Santoni et al., 2002).

The model predicts the increase of upward gas velocity in the combustion zone caused by buoyancy forces. In the preheating zone, the predicted upward gas velocity decreases ahead of the fire-front but is not nil due to gradient between the temperature of the bed of fuel and the temperature of the ambient air. The horizontal gas velocity distribution exhibits a slight acceleration, before penetrating the flame zone due to the aspiration of cold gas; this phenomenon is enhanced with increasing wind velocity. Then, it decreases rapidly as it goes through the combustion zone. The horizontal component, which keeps a non nil value ahead of the fire-front, combined with the temperature gradient are responsible for the preheating by forced convection. A gas outlet through the combustion zone has always been predicted regardless of the wind

velocity entering this zone and no fresh gas inlet from the preheating zone was observed for lower wind velocities. This observation remains to be verified experimentally.

<u>Heat flux contribution</u>

A qualitative study of heat fluxes received ahead of the fire-front is provided hereafter in order to estimate predicted fraction of radiation and convection in total heat transfer. Heat fluxes distribution patterns at the centreline of the bed are plotted in Figure 10 for wind blown fire spread across a 10° up-slope. These distribution patterns are provided for 1 $m.s^{-1}$ and 2 $m.s^{-1}$ at times 100 and 55 s, respectively. Concordant fire-front shapes are provided in Figure 8. Radiative and convective contributions are the most representative of fire spread under wind and slope conditions. Thus, contribution of the diffusion term in the energy conservation equation is not significant under these conditions and will not be discussed here.

The distance of preheating of the unburned fuel located ahead of the fire-front and total heat flux impinging on it increase with increasing wind. Impact of radiation (due to flame tilt) acts over a great distance from the fire-front. On the other hand, the amount of energy transferred through the bed of fuel by convection is received closer to the front. These last results are in agreement with the predictions of the multiphase approach of Porterie et al. (2000). As a result, about 40% of total energy is received over a distance of 10 cm from the front.

By integrating these fluxes over the preheating region, for a 1 $m.s^{-1}$ wind blown fire across a 10° sloping bed, the predicted amount of energy received by radiation and convection are 1112 W and 486 W, respectively. For a 2 $m.s^{-1}$ wind blown fire, these values are 1679 W and 762 W, respectively. Model predictions indicate that radiation is the predominant preheating mechanism with a significant contribution from convection.

These results are in agreement with the predictions of the Pagni and Peterson model (1973) on pine needle beds. For instance, during horizontal and 10° up-slope spread of the fire under 2 $m.s^{-1}$ wind velocity, the radiation represents 60% and 70% of the total heat transfer, respectively. Nevertheless, forced convection dominates near the combustion region due to high temperature gradient. The overall pattern remains to be verified experimentally.

CONCLUSION

Improvements of the modelling of the effects of wind and slope with regard to our earlier work, including both flame radiation and forced convection during the fuel-bed preheating process, have been presented. The model predictions are now able to account of the rate of spread even for the high wind velocities.

The amount of radiation impinging on the top of the bed of fuel depends on flame properties which are an input of the model. Under zero slope condition, the characteristics flame length scales for spreading line-fire across pine needles bed, have been estimated from image processing. The use of the infrared technique can give more accurate results than standard video technique which is based on luminous intensity of the images. Standard video technique is less appropriated to localise flame region than the one presented in this paper. Indeed, a thermal criterion was used (since infrared images represent local flame radiation intensity) instead of an optical criterion. Thus, there is no limitation due to luminous intensity or colour of the flame. Empirical correlations, established for static fires by McCaffrey, have been used successfully to determine centreline temperature and velocity??? distributions for a spreading line fire. This technique provided good results but remains to be tested in other laboratories conditions (wind and slope) and under a more realistic scale.

This work underlines also the importance of carrying out specific experimentation in order to validate the predictions of the models. The use of infrared thermography allowed put to the fore that the thermal equilibrium between solid and gaseous phases is not achieved during pyrolysis and this non-intrusive measuring technique have to be developed. Analysis of the temperature curves also indicated that solid degradation processes have to be considered independently in the model. For horizontal fire spread in still air, the heat flux measurements allowed to validate the part of radiation and impinging ahead of the fire front predicted by the model.

Under wind-blown conditions, the model predictions of the rate of spread are in good agreement with observations when direct flame contact on the bed of can be neglected. The effects of wind and slope on fuel-bed temperature have been qualitatively predicted. The fire-front curvature increase and fire-front rate of spread increase with increasing wind and slope have also been predicted. The qualitative study of the relative importance of radiation and convection heat fluxes ahead of the fire-front was presented. For the range of wind velocities considered, predictions showed that fire spread is mainly controlled by the amount of radiant energy transferred from the flame to the unburned fuel with a significant contribution of convection. Nevertheless, these predictions remains to be tested against experimental data.

A certain number of improvements must be made, however, before the model can be used in the battle against forest fires. As far as flame radiation modelling is concerned, it could be improved taking into account the temperature dependence with height. Furthermore, flame characteristics such as length and tilt angle, were assumed to be known *a priori* and predictions of these quantities would be of great interest. The simplified flow modelling can also be improved, in order to describe two-dimensional

25

flow in the fuel layer. The influence of the flow have to be considered not only by increasing the thermal transfers but also by increasing the reaction kinetic.

The present approach was relevant at laboratory scale but future research will need to include the simulation of forest fire spread under full-scale complex topographical conditions in order to provide a fire management tool.

NOMENCLATURE

a	absorptivity
B	Stefan-Boltzmann constant
C_p	Specific heat at constant pressure
h	Reduced cooling convective coefficient
k	reduced forced convection coefficient
K	Reduced diffusion coefficient
m	Thermal mass per unit area
Q	Reduced combustion enthalpy
r	distance between an elementary surface element of the flame and an elementary surface element of the bed of fuel
R	Reduced radiant energy flux
s	Angle of slope
S	Surface
t	Time
T	Temperature
n	Normal unit vector
V	Velocity inside the bed of fuel

Greek symbols

α Volume fraction

Δ Laplacian in two-dimensional Cartesian coordinates

χ Drag forces coefficient

δ Fuel-bed thickness

ε Emissivity

ϕ Radiant heat flux absorbed by a fuel element

γ Combustion time constant

φ Angle in the view factor calculation

ρ Density

σ Surface mass

Subscripts

0 Initial condition

a Ambient

fl Flame

g Gas phase

ig Ignition

k Solid phase

w Wind

x Horizontal component

z Upward component

REFERENCES

Balbi J.H., Santoni P.A., Dupuy J.L., Int. J. of Wildland Fire 9 (1999) 275-284.

Catchpole W.R., Catchpole E.A., Butler B.W., Rothermel R.C., Morris G.A., Latham D.J., Combust. Sci. Tech. (131) (1998) 1-37.

Catchpole W.R., Catchpole E.A., Tate A.G., Butler B. and Rothermel R.C. (2002) A model for the steady spread of fire through a homogeneous fuel bed. . IV Int. Conf. on Fire Research, Luso.

Cheney N.P., 'Fire behaviour.' in A. M. Gill, R. H. Groves, and I. R. Noble (eds.), Fire and the Australian Biota, Australian Academy of Science, Camberra, 1981, 151-175.

Den Breejen E., Roos M., Schutte K., De Vries J.S., Winkel H., III Int. Conf. on Fire Research, Luso, VOL I, (1998) 517-532.

Dupuy J.L., Int. J. of Wildland Fire 5 (3) (1995) 153-164.

Dupuy J.L., Maréchal J., Bouvier L., Lois N., III Int. Conf. on Fire Research, Luso, VOL I, (1998) 843-858.

Fons W.L., Journal of Agricultural Research (13) (1946), 93-121.

Grishin A.M., Mathematical modeling of forest fires and new methods of fighting them. Publishing house of the Tomsk state university, Albini, 1997.

Larini M., Giroux F., Porterie B., Loraud J.C. Int. Journal of Heat and Mass Transfer, 41(6-7) (1997) 881-897.

Linn R.R., Harlow F., III International Confer. on Fire Research, Luso, VOL I, (1998) 363-372.

Margerit J., Séro-Guillaume O., Int. Journal of Heat and Mass Transfer, 45(8) (2002), 1723-1737.

McCaffrey B.J. 1979. Purely buoyant diffusion flame: some experimental results, *NBSIR* 79-1910.

Mendes-Lopes J.M., Ventura J.M., Amaral J.M., III Int. Confer. on Fire Research, Luso, VOL I, (1998) 497-511.

Morandini F., Marcelli T., Rinieri F. and Balbi J.H. "Measurement of Pine Needles Buoyant Diffusion Flame Characteristics Using Infrared Technique". IV International Conference on Forest Fire Research, Coïmbra Portugal, (2002)

Morandini F., Santoni P.A., Balbi J.H., Combust. Sci. and Tech, 166 (2001a) 67-90.

Morandini F., Santoni P.A., Balbi J.H., Fire Safety J. 36 (2001b) 519-543.

Pagni P.J., Peterson T.G., 14th Int. Sym. on Combust. The Combustion Institute, Pittsburg (1973) 1099-1107.

Porterie B., Morvan D., Loraud J.C., Larini M., Physics of fluids, 12 (7) (2000), 1762-1782.

Rothermel R.C., A mathematical model for predicting fire spread in wildland fuels. United States Department of Agriculture, Forest Service Research INT-115 (1972).

Santoni P.A., Balbi J.H., Dupuy J.L., Int. J. of Wildland Fire 9 (1999) 285-292.

Santoni P.A., Marcelli T., Leoni E., Combust. Flame 131 (1-2) (2002), 47-58.

Simeoni A., Santoni P.A., Larini M., Balbi J.H., Comb. Sci. and Tech. 162 (2001) 59-84.

Simeoni A., Larini M., Santoni P.A., Balbi J.H., C. R. Mécanique 330 (2002) 783-790.

Simeoni A., Santoni P.A., Larini M., Balbi J.H., Int. J. of Thermal Sci.42 (2003) 95-105.

Steward F.R., Fire spread through a fuel-bed. Heat transfer in fires, chap 2, (1974) 315-378.

Vaz G.C., André J.C.S. and Viegas D.X. (2002) Modelling the spread of a straight fire front through a horizontal porous fuel bed without wind. IV Int. Conf. on Fire Research, Luso.

Ventura J.M., Mendes-Lopes J.M., Ripado L.M. III Int. Conf. on Fire Research, Luso, VOL I, (1998) 699-711.

Viegas D.X., Forest fire propagation, Phil. Trans. R .Soc. Lond. A 356 (1998) 2907-2928.

Viegas D.X., Varela V.G., Borges C.P., II Int. Confer. on Fire Research, Luso, VOL. I, B.11 (1994) 301-318.

Weber R.O., Combust. Flame 78 (1989) 398-408.

Weise D.R., Biging G.S., Forest Science 43(2) (1997) 170-180.

Table 1. Model parameters for a bed of *Pinus pinaster* needles (fuel load of *0.5 kg.m^{-2}* and moisture content of *10 %*)

model parameter	h (s^{-1})	$\underline{K}$ $(m^2.s^{-1})$	Q $(m^2.K.kg^{-1})$	γ (s^{-1})
value	$41{\times}10^{-3}$	$13{\times}10^{-6}$	$2.34{\times}10^{3}$	0.35

Table 2. Sensibility of the heat flux sensors

	Heat fluxes	Sensibility $(\mu V/(W/m^2))$
Sensor	Convective	0.707
	Radiant	0.374
Sensor	Convective	0.566
	Total	0.561

Table 3. Empirical coefficient for McCaffrey correlations

Flame zone	η	K_T	K_V
Continuous	$\dfrac{1}{2}$	$\left(\dfrac{k}{C}\right)^2$	k
Intermittent	0	$\dfrac{2g\Delta T_c}{T_0}\times\dfrac{L_c}{Q^{2/5}}$	$\dfrac{V_c}{Q^{1/5}}$
Plume	$-\dfrac{1}{3}$	$\dfrac{2g\Delta T_c}{T_0}\times\dfrac{L_c}{Q^{2/5}}\times\left(\dfrac{L_m}{Q^{2/5}}\right)^{2/3}$	$\dfrac{V_c}{Q^{1/5}}\times\left(\dfrac{L_m}{Q^{2/5}}\right)^{1/3}$

where k is coefficient for center line correlations ($k = 6.9$); C = buoyancy constant ($C = 0.9$).
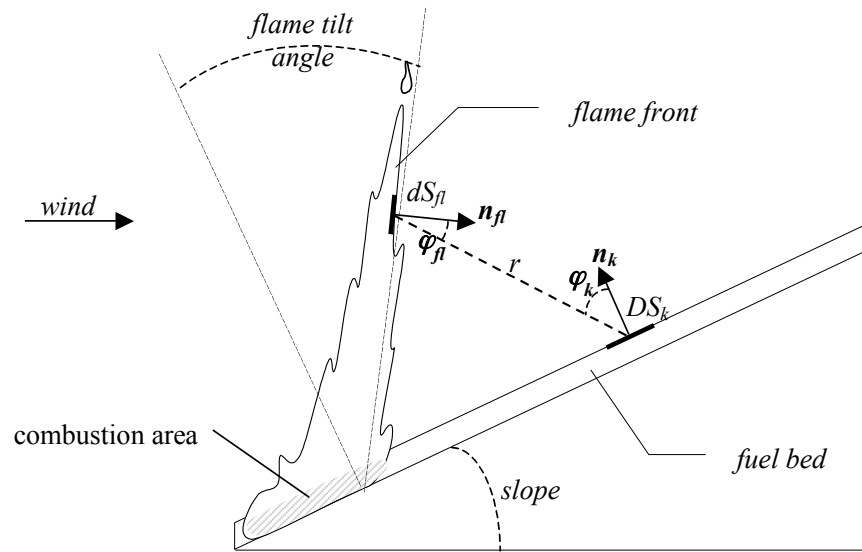
Figure 1. Radiative transfers between two elementary surfaces
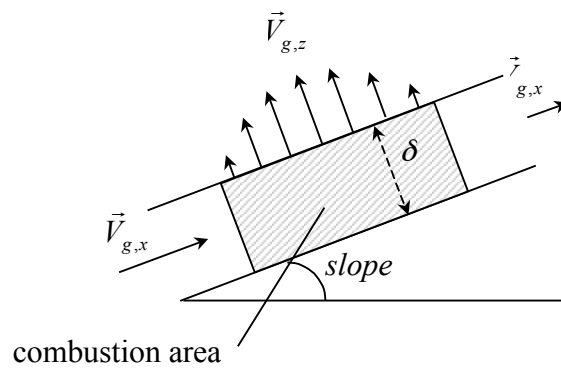
Figure 2. Schematic representation of the flow within the fuel layer
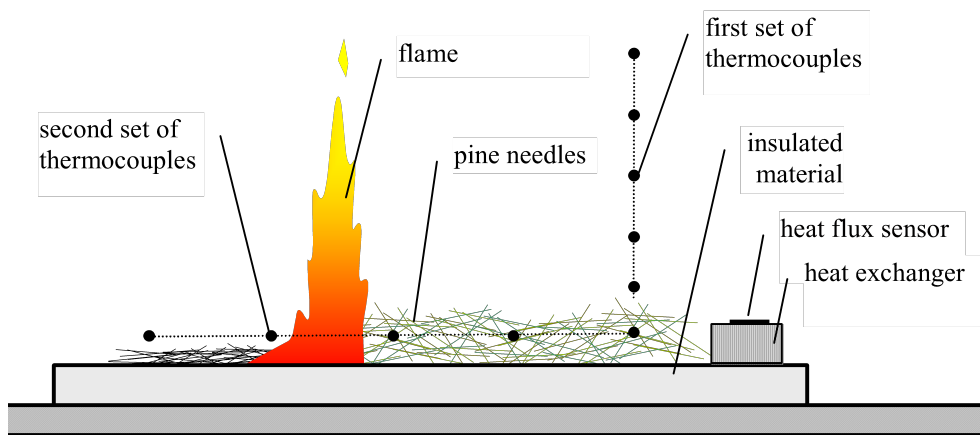
Figure 3. Sketch of experimental apparatus, for horizontal fire spread across a pine needles bed in still air
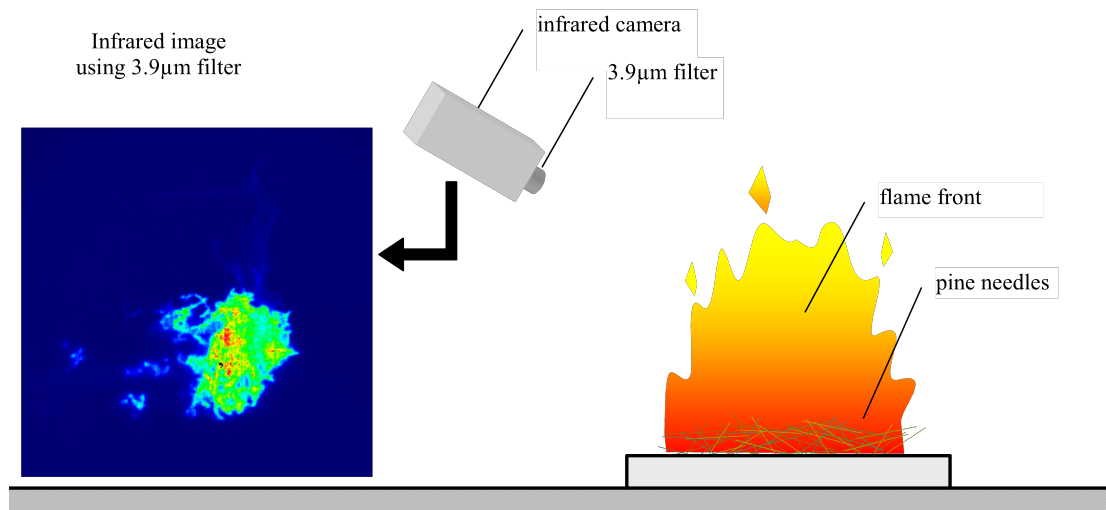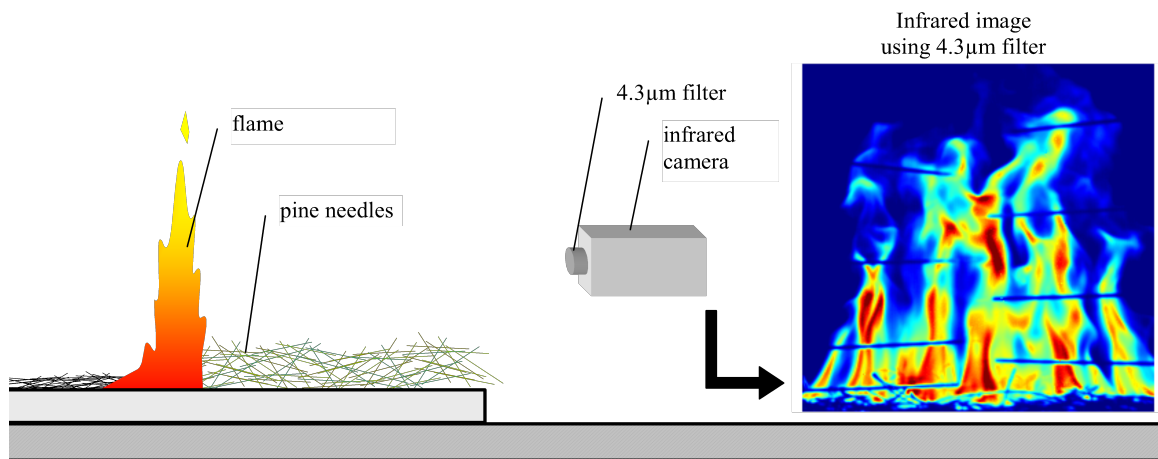
Figure 4. Location of the infrared camera for combustion measurements (a) in the gaseous phase (b) in the solid phase
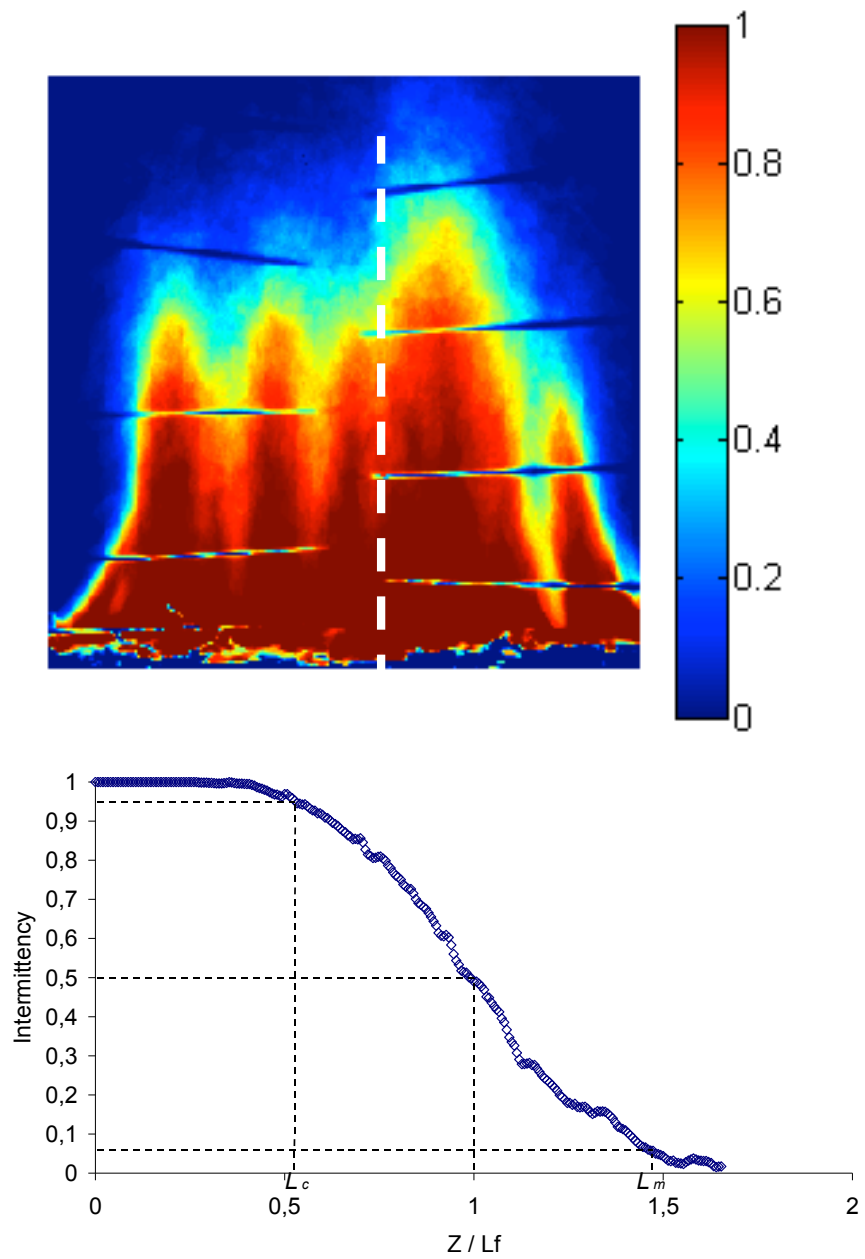
Figure 5. Fire spread across a pine needles bed (a) Flame presence probability contours and (b) intermittency of flame at the centreline of the flame front
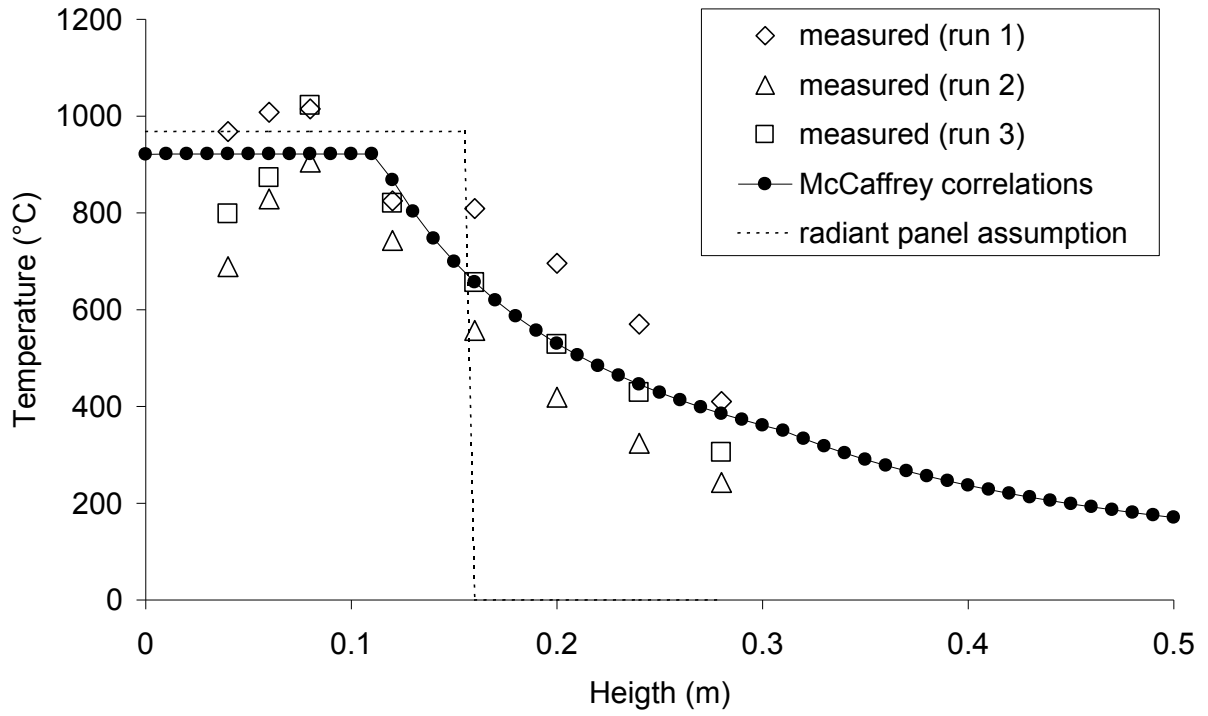
Figure 6. Comparison between predicted and measured centreline temperature distribution for fire spread across a pine needles bed
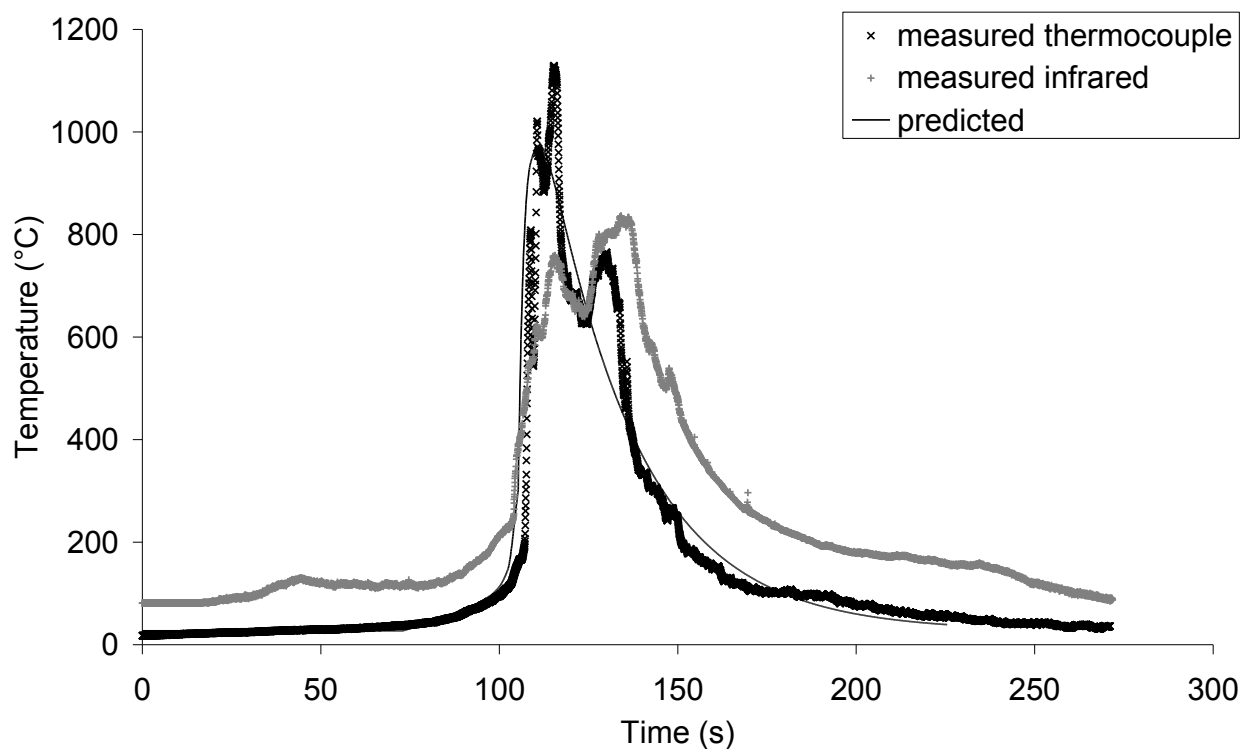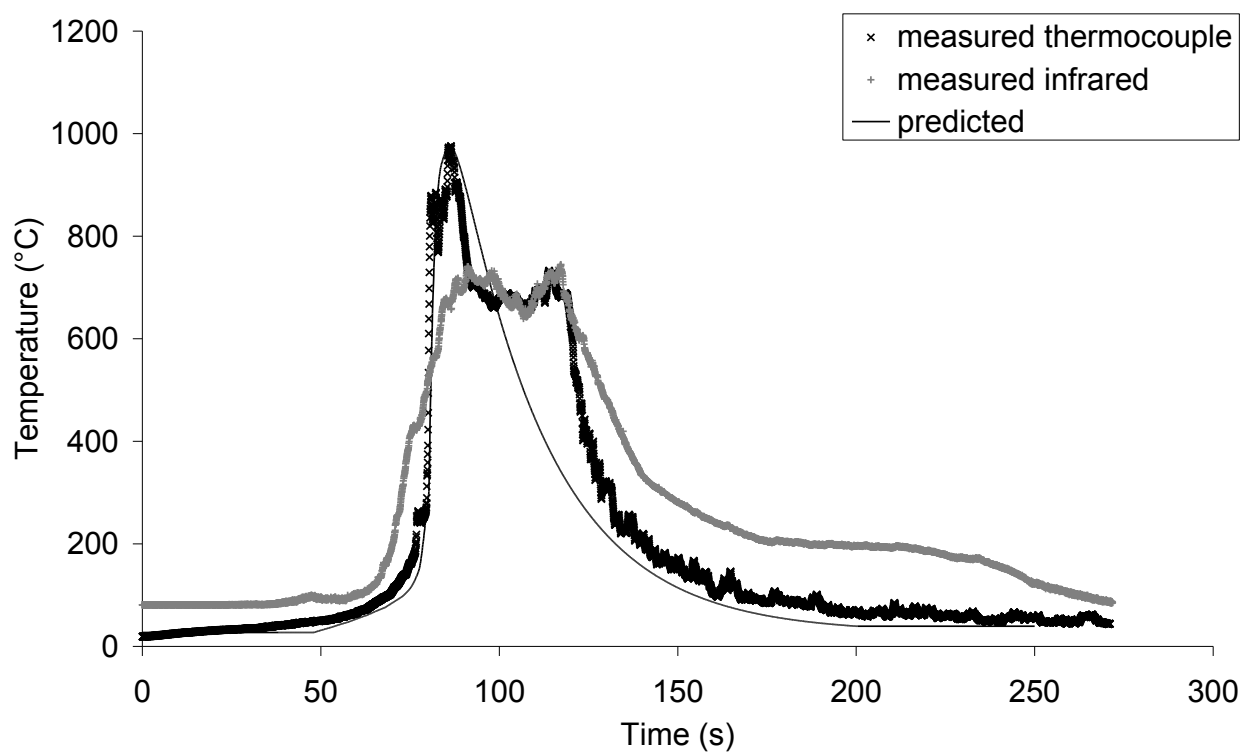
Figure 7. Comparison between predicted and measured temperature-time curves , for horizontal fire spread across a *0.5 kg.m⁻²* load of *Pinus pinaster* needles
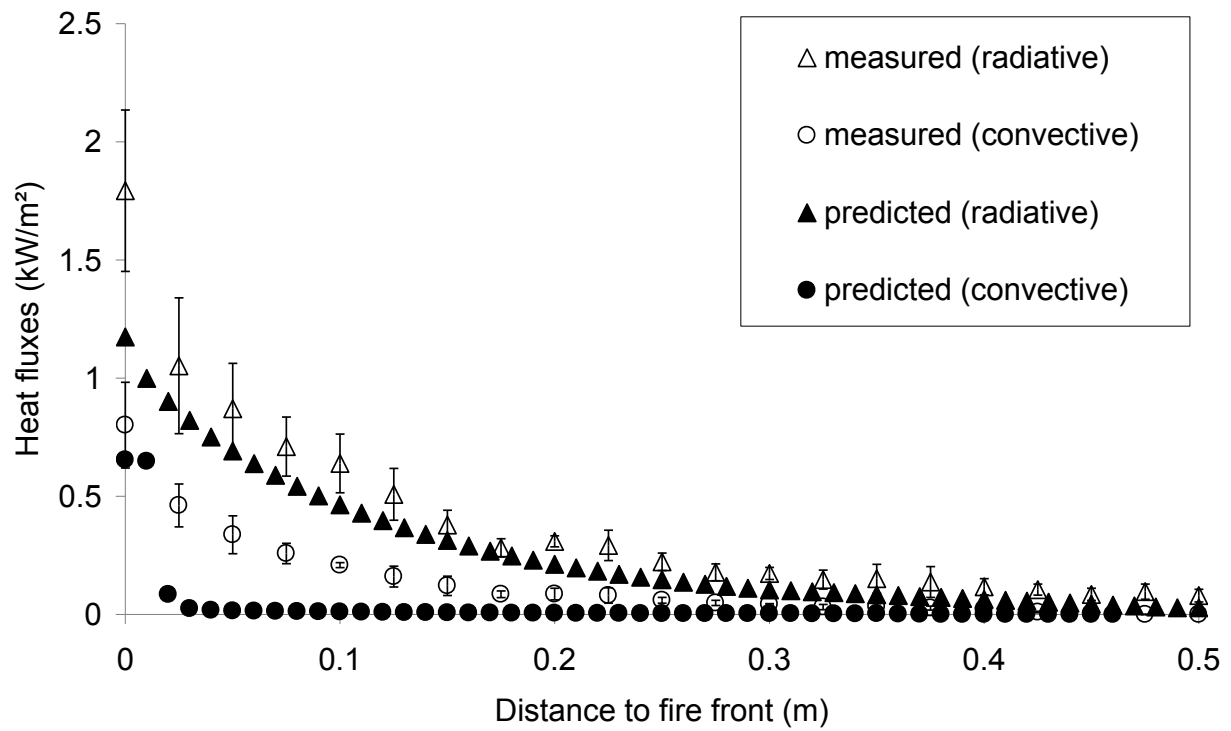
Figure 8. Heat fluxes received upon the top of the bed of pine needles for horizontal fire spread
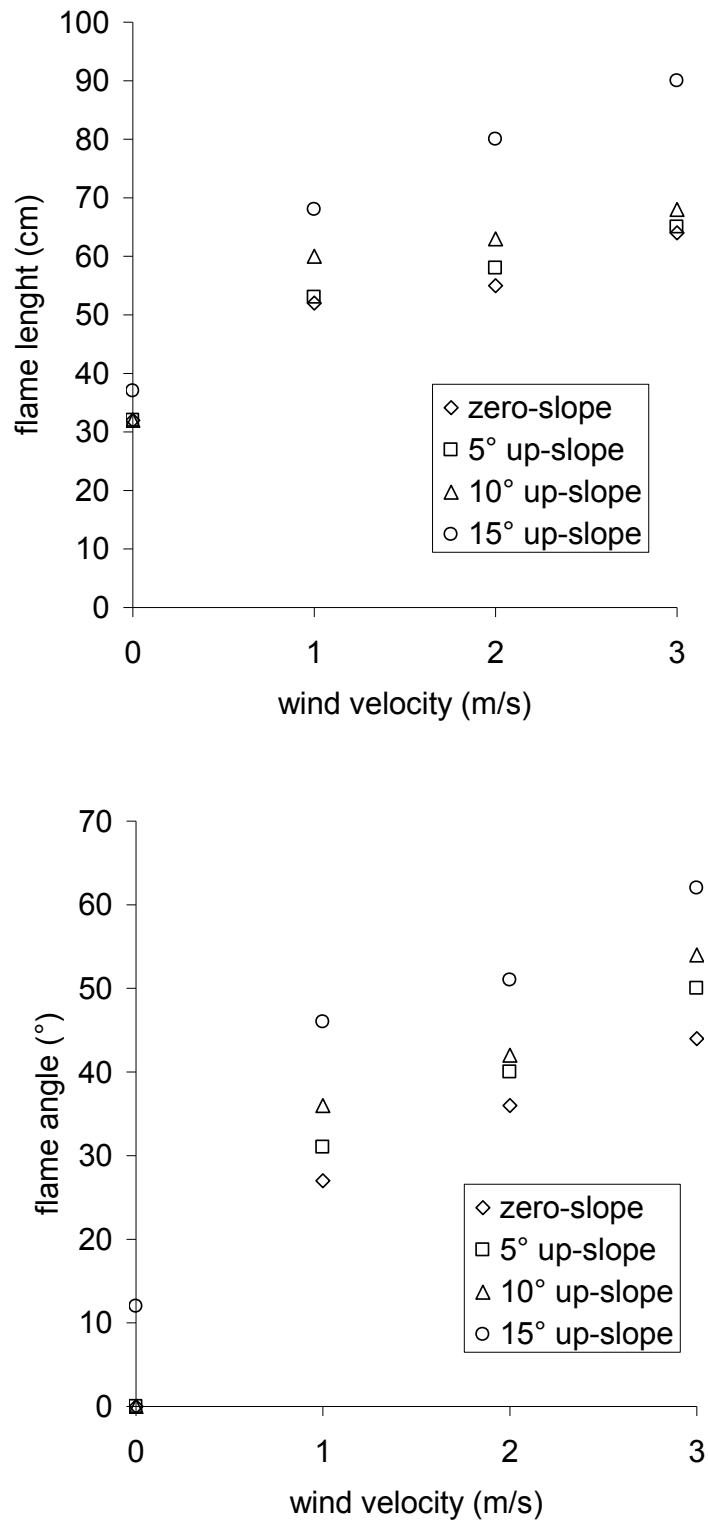
Figure 9. Influence of wind and slope on flame properties : (a) flame length, (b) flame tilt angle

40
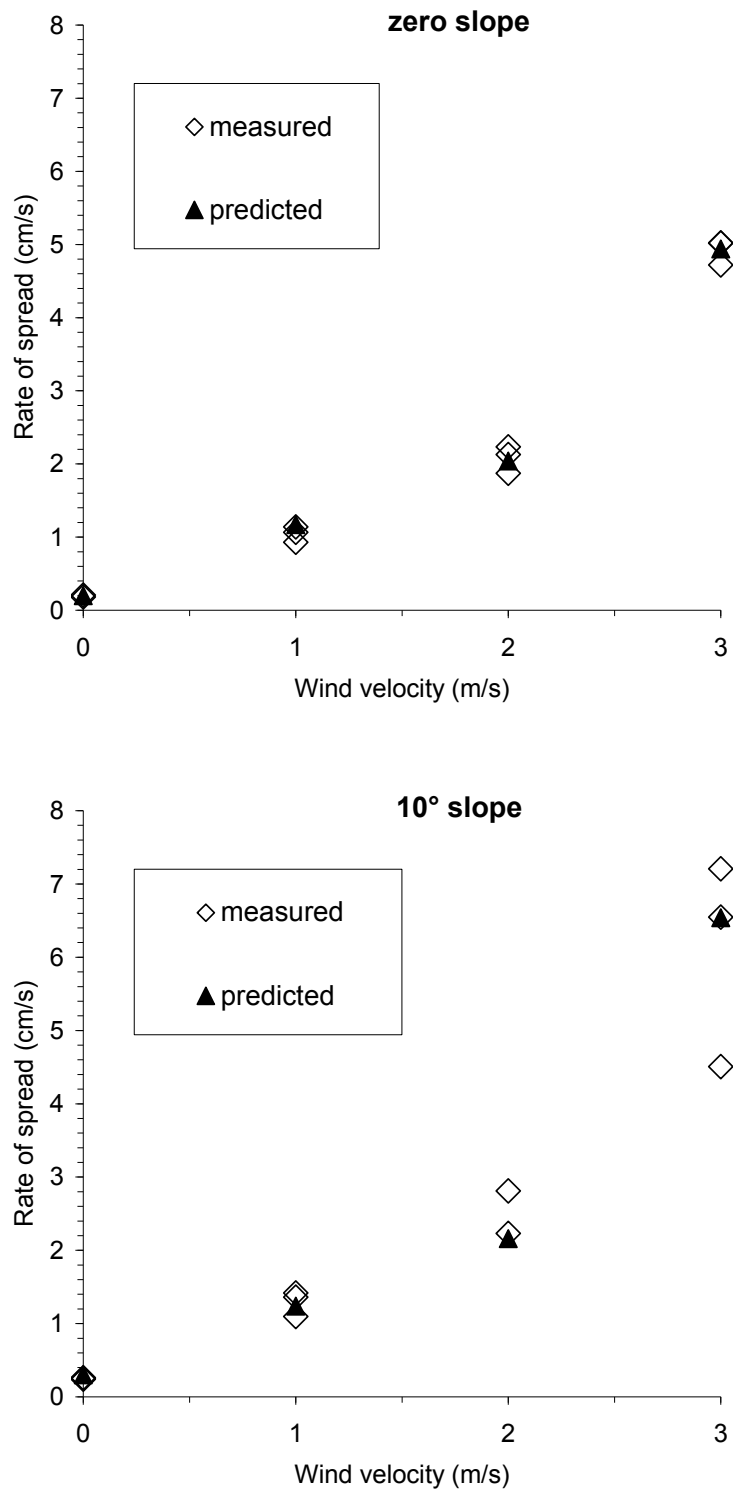
Figure 10. Predicted and observed rate of spread ($cm.s^{-1}$), for wind-blown fire spread across a *0.5 kg.m^{-2}* load of *Pinus pinaster* needles : (a) zero slope, (b) 10° up-slope
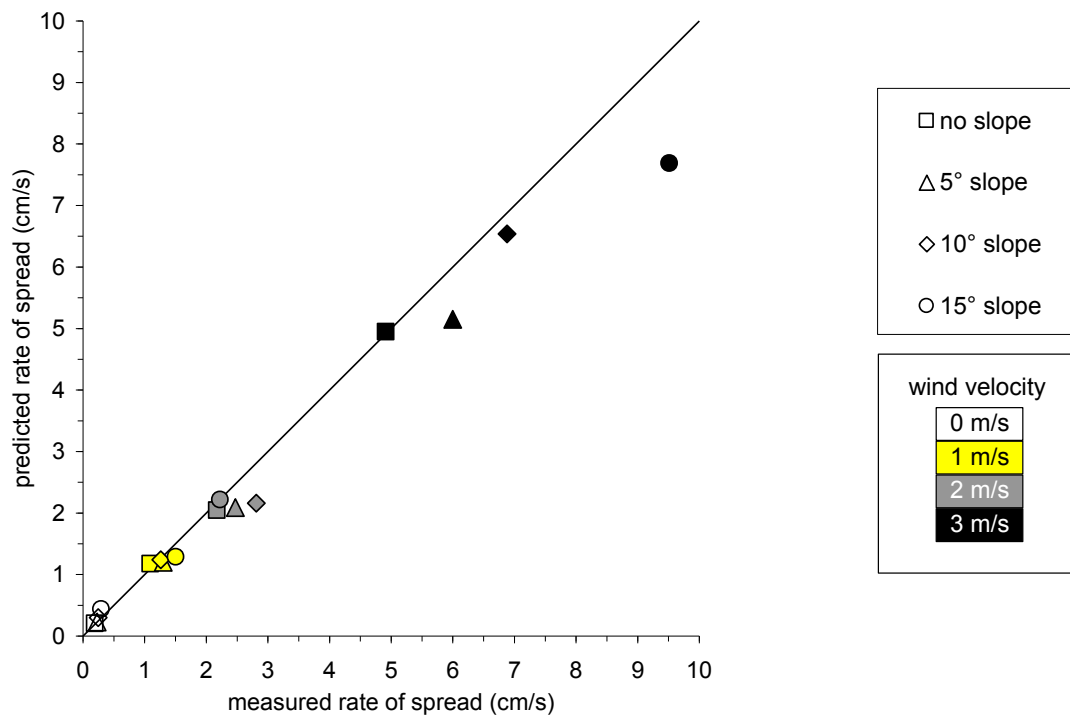
Figure 11. Predicted versus observed rate of spread ($cm.s^{-1}$), for up-slope fire spread under wind conditions across a *0.5 kg.m^{-2}* load of *Pinus pinaster* needles
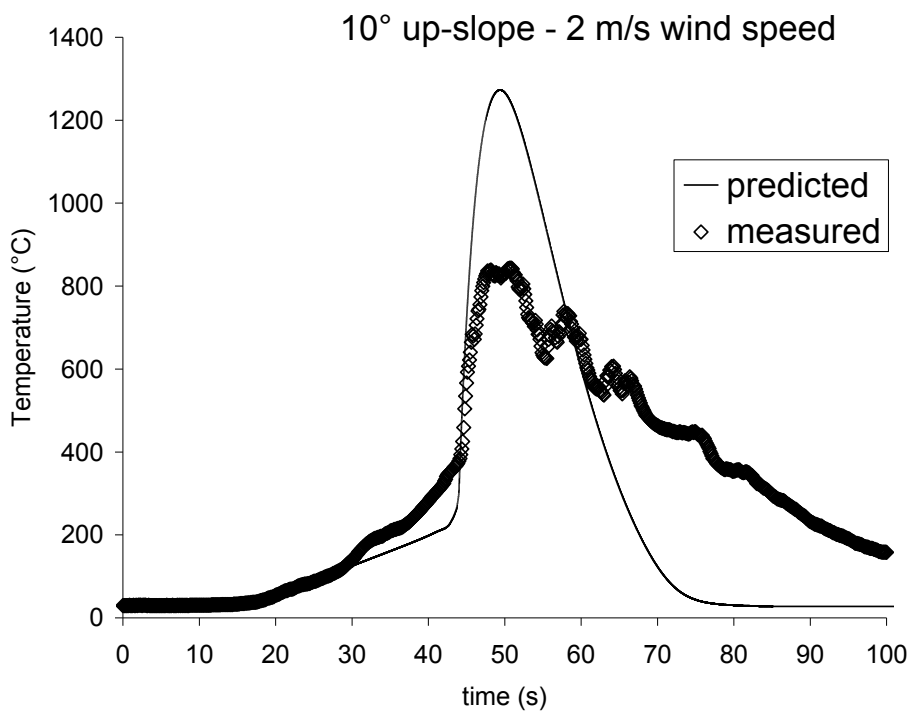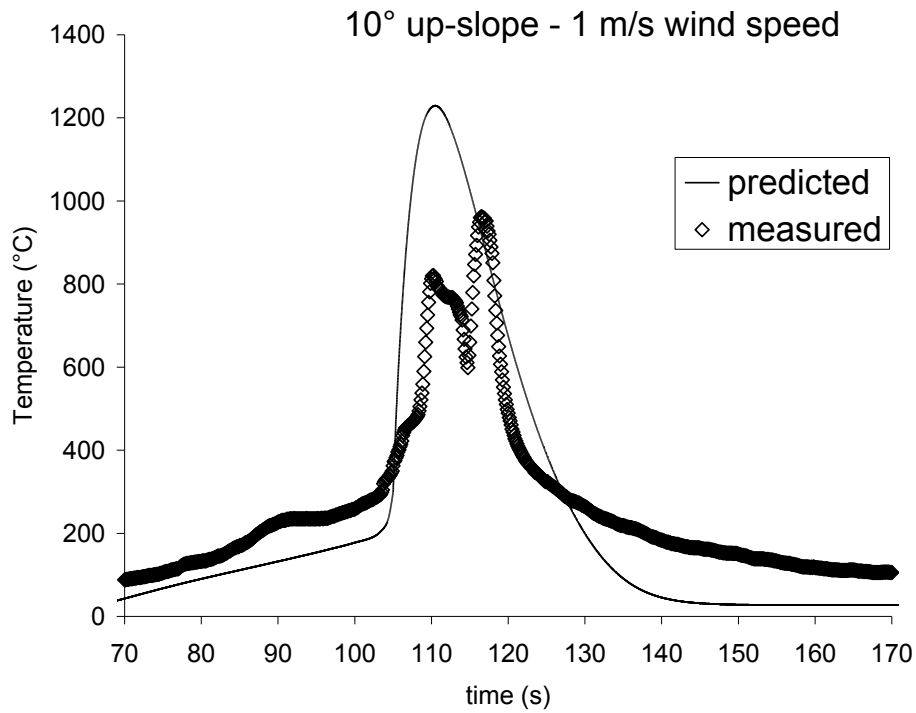
Figure 12. Predicted and observed temperature-time curves, for *10°* up-slope and wind-blown fire spread across a *0.5 kg.m⁻²* load of *Pinus pinaster* needles : (a) wind velocity *1 m.s⁻¹*, (b) wind velocity *2 m.s⁻¹*
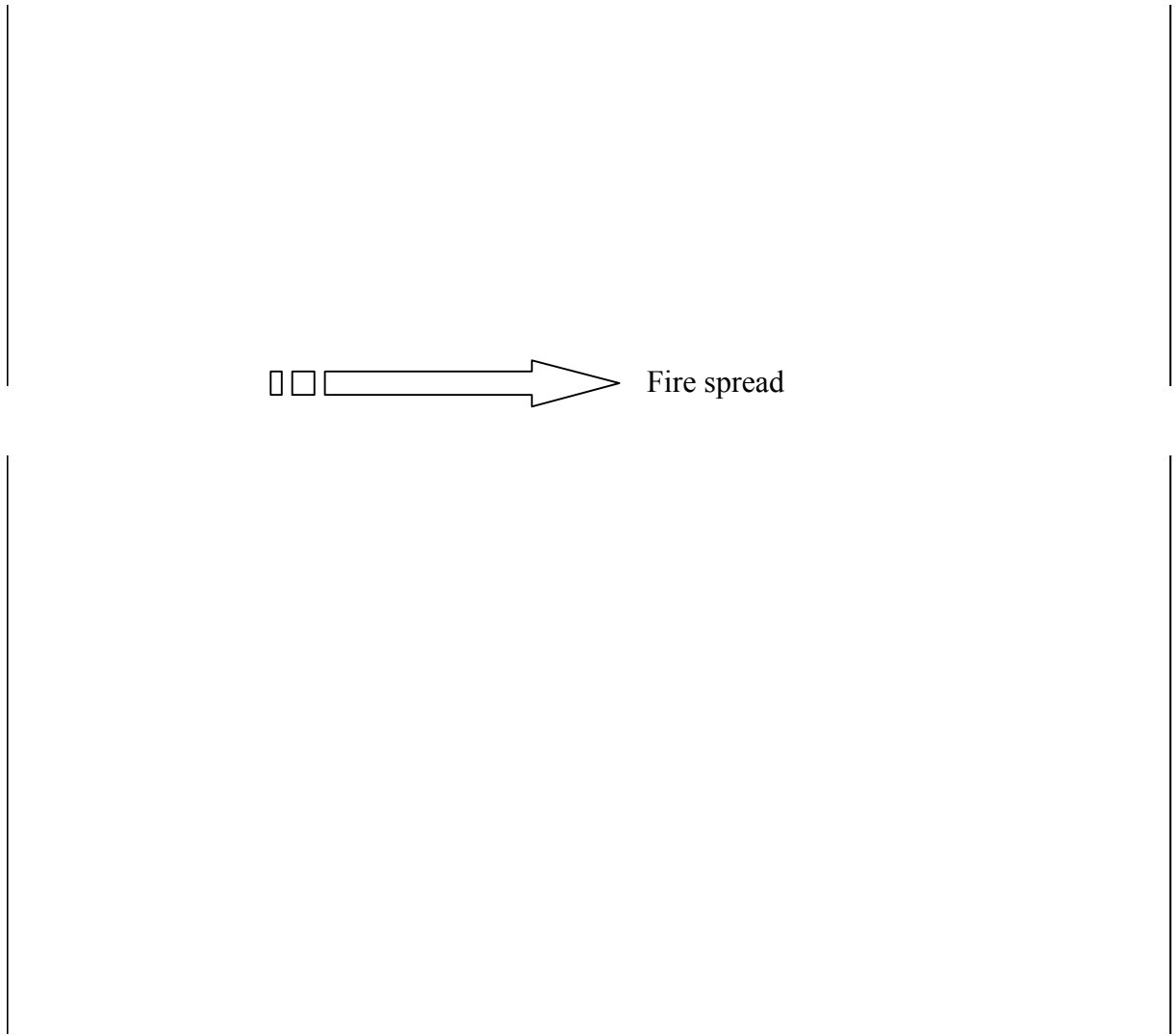
Fire spread

Figure 13. Predicted temperature contours (*°C*) for *10°* up-slope and wind-blown fire spread across a *0.5 kg.m^{-2}* load of *Pinus pinaster* needles : (a) wind velocity *1 m.s^{-1}* (at time *100 s*), (b) wind velocity 2*m.s^{-1}* (at time *55 s*)
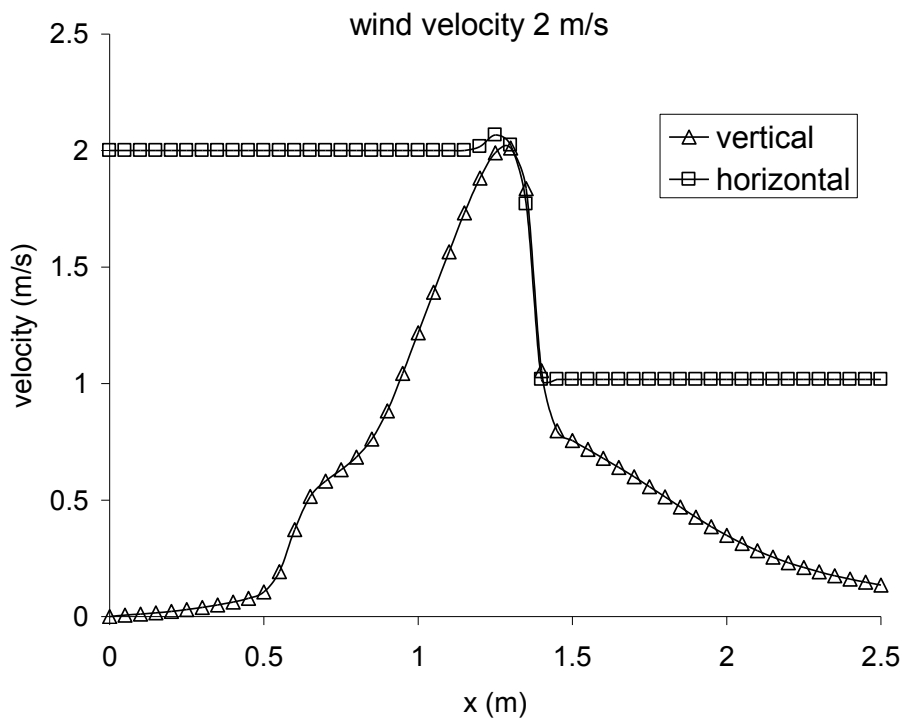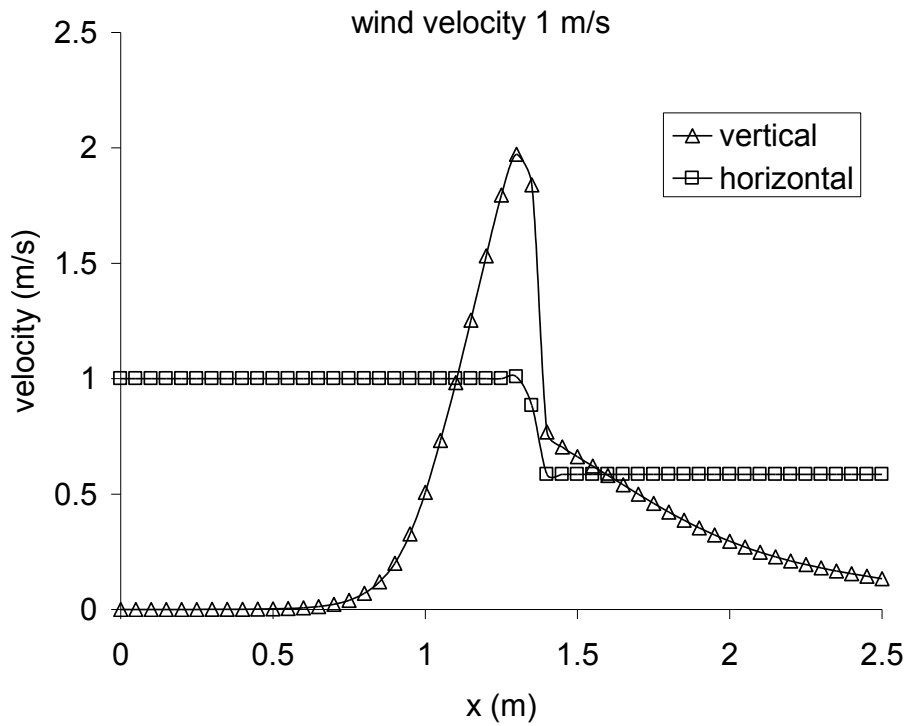
Figure 14. Predicted velocity components inside the fuel bed ($m.s^{-1}$), for 10° up-slope and wind-blown fire spread across a *0.5 kg.m^{-2}* load of *Pinus pinaster* needles : (a) wind velocity *1 m.s^{-1}* (at time *100 s*), (b) wind velocity *2 m.s^{-1}* (at time *55 s*)
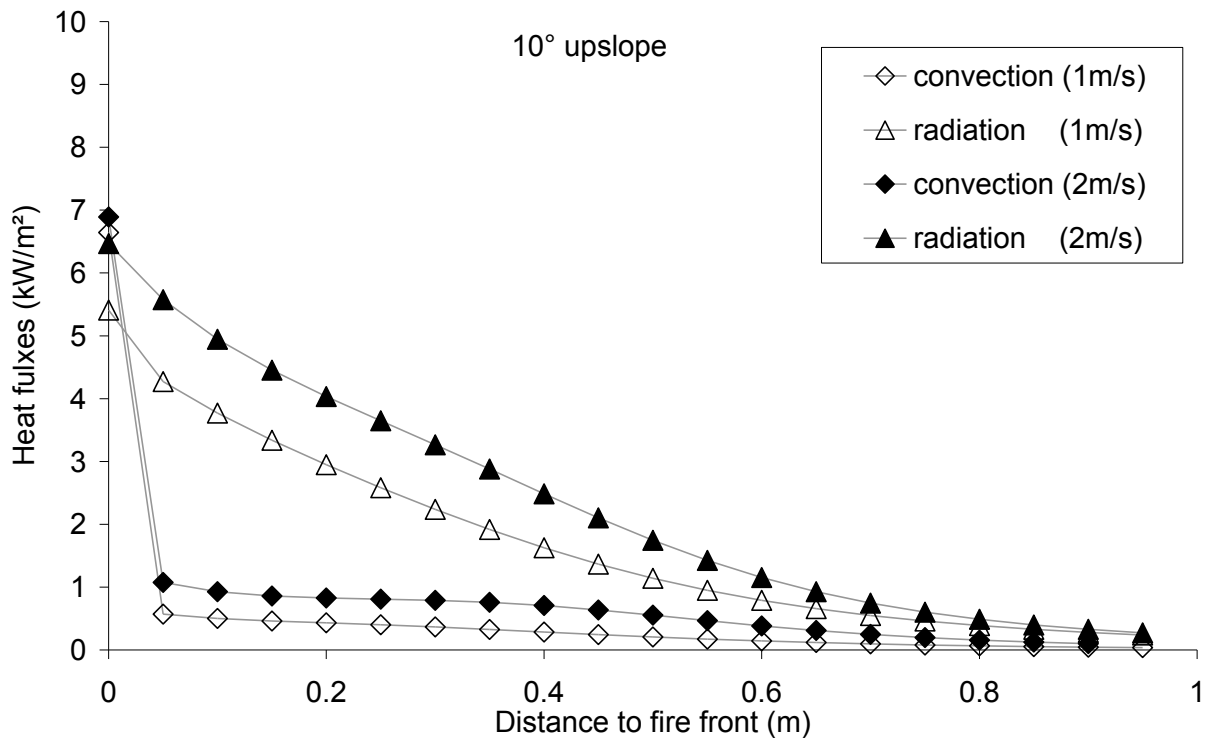
Figure 15. Predicted heat flux distributions (*W.m⁻²*) ahead the fire front for *10°* up-slope and wind-blown fire spread across a *0.5 kg.m⁻²* load of *Pinus pinaster* needles : (a) wind velocity *1 m.s⁻¹*, (b) wind velocity *2 m.s⁻¹*